Plasma removal of Parylene C

Ellis Meng[1], Po-Ying Li[2] and Yu-Chong Tai[3]

[1] Department of Biomedical Engineering, University of Southern California, 1042 Downey Way,
DRB-140 Los Angeles, CA 90089-1111, USA
[2] Department of Electrical Engineering, University of Southern California, 3737 Watt Way,
PHE-604 Los Angeles, CA 90089-0271, USA
[3] Department of Electrical Engineering, California Institute of Technology, 1200 E California Blvd.,
Pasadena, CA 91125, USA

E-mail: ellis.meng@usc.edu

Abstract
Parylene C, an emerging material in microelectromechanical systems, is of particular interest
in biomedical and lab-on-a-chip applications where stable, chemically inert surfaces are
desired. Practical implementation of Parylene C as a structural material requires the
development of micropatterning techniques for its selective removal. Dry etching methods are
currently the most suitable for batch processing of Parylene structures. A performance
comparison of three different modes of Parylene C plasma etching was conducted using
oxygen as the primary reactive species. Plasma, reactive ion and deep reactive ion etching
techniques were explored. In addition, a new switched chemistry process with alternating
cycles of fluoropolymer deposition and oxygen plasma etching was examined to produce
structures with vertical sidewalls. Vertical etch rates, lateral etch rates, anisotropy and sidewall
angles were characterized for each of the methods. This detailed characterization was enabled
by the application of replica casting to obtain cross sections of etched structures in a
non-destructive manner. Application of the developed etch recipes to the fabrication of
complex Parylene C microstructures is also discussed.

(Some figures in this article are in colour only in the electronic version)

1. Introduction

Parylene, or poly (*p*-xylylene), is one of the most well-known
chemical vapor deposited (CVD) thin film polymers. It is
used in a wide range of applications, particularly as a coating
for biomedical implants and microelectronics. Its desirable
properties include chemical inertness, conformal coating and
excellent barrier properties [1]. Originally discovered in
1947 by Swarc, Parylenes were not commercialized by Union
Carbide until 1965 following the development of a CVD
polymerization process by Gorham [2–4]. Although over
twenty types of Parylene have been developed, only three
are commonly available: Parylenes N, C and D (figure 1).
With increasing interest in Parylenes, newer commercial
products have recently been introduced including, Parylene HT
(Specialty Coating Systems, Indianapolis, IN), a fluorinated
version of the polymer, and diX A and AM (Kishimoto Sangyo
Co., Ltd, Japan), having amino groups attached to the benzene
rings.

Parylene C (poly(monochloro-*p*-xylylene)) has a long
history of use in the medical industry as a coating for
stents, cardiac assist devices, surgical tools, electronics and
catheters [5]. The use of Parylene C as a structural material
in microelectromechanical systems (MEMS) devices and in
particular bioMEMS and microfluidics has gained traction
[6–10]. Among the many polymers used as structural
materials, Parylene C is an increasingly popular choice due to
its deposition method, low process temperature, transparency
and compatibility with standard microfabrication processes
[11]. It is possible to perform multilayer processing of
Parylene films to produce complex structures and devices.

Parylene C is a USP (United States Pharmacopeia)
Class VI polymer. This designation is the highest level of
biocompatibility possible for polymers permitting its use in
applications where long-term implantation is required. Its
biocompatibility, biostability, low cytotoxicity and resistance
against hydrolytic degradation [1, 12, 13] have resulted
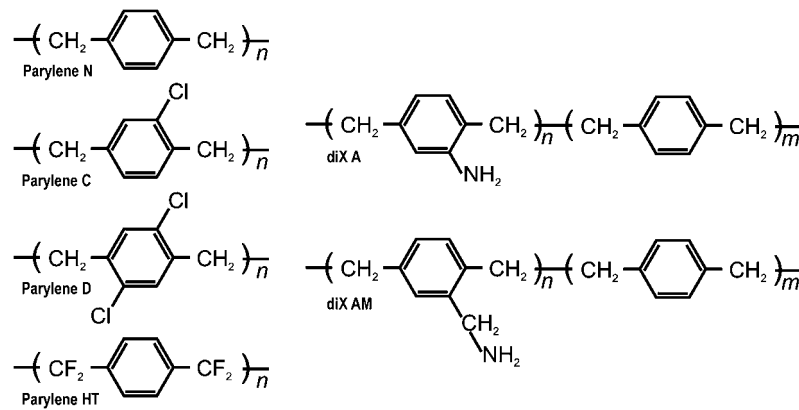in increasing popularity of Parylene C in micro- and

Figure 1. Commercially available poly (*p*-xylylene) types.

nano-fabricated devices for microfluidic and bioMEMS applications. For example, Parylene C-based devices have been demonstrated as platforms for neuronal growth [14–16] and in implantable neuronal probes [17]. Furthermore, new developments on the functionalization of Parylene surfaces may expand its use in biomedical applications [18–20].

Pattern transfer of masks into Parylene C films is a critical enabling step in Parylene microfabrication technology. Dry plasma-based etching techniques are likely the most suitable means for achieving fine features in Parylene C films. The characterization of Parylene C removal by oxygen-based plasmas was investigated for three plasma etching modes: plasma, reactive ion and deep reactive ion etching. In particular, the focus of this study was on identifying process parameters that will enable anisotropic etching toward achieving high aspect ratio (HAR) structures desirable for MEMS applications. Removal rates for the photoresist masking layer were also monitored.

2. Patterning Parylene

2.1. Chemical removal

A key feature of Parylene is chemical inertness which complicates its chemical removal. Below the melting point, Parylene is resistant to dissolution by solvents. At temperatures above 150 °C, it is possible to remove Parylene in either chloronaphthelene or benzolyl benzoate [21]. However, this method is not compatible with most commonly used lithographic processes. The highly conformal natural of Parylene films prevents patterning via lift-off processes.

2.2. Plasma removal

Oxygen (O_2) plasmas are used to etch many polymers but the specific mechanisms for this removal are not well understood. Polymer etching in pure oxygen plasmas is linked to the presence of atomic O; etching enhancement is associated with an increase in atomic O by increase of dissociation, reduction of losses due to recombination, and increase of O atom flux from the plasma to the sample [22]. Increases in electron density or electron energy can increase O_2 dissociation.

Parylene is readily removed in oxygen-based plasmas and the possible etching reactions that govern Parylene removal have been suggested [23, 24]. The etching mechanism for Parylene C is thought to be similar to that of Parylene N which is different only by the absence of a chlorine atom. Plasma removal of Parylene N is attributed to the opening of the benzene ring which is necessary in etching of aromatic polymers. This process is thought to occur as follows. First, hydrogen is abstracted by an oxygen radical from the ethyl carbons between the benzene rings in the polymer chain and a hydroxyl radical is formed. Then the exposed reactive site is subjected to molecular or atomic oxygen absorption to form an unstable peroxy radical. Rearrangement of the unstable species can then result in the formation of volatile carbon monoxide (for atomic oxygen adsorption) or carbon dioxide (for molecular oxygen adsorption). Further oxygen attack on the radical site results in ring opening.

While the mechanisms governing Parylene C removal are likely similar to those for Parylene N, the presence of a chlorine atom on the ring reduces the available reactive carbon sites by one. If ring opening is the rate limiting step in Parylene etching, then the reduction in reactive sites may explain the observed reduction in Parylene C etch rate compared to that of Parylene N by ~17% [23].

Parylene etching has been demonstrated in multiple modes including plasma etching [19, 25, 26], reactive ion beam etching (RIBE) [27], reactive ion etching (RIE) [28, 29] and high-density plasma etching [30]. However, no attempt has been made to optimize anisotropy or employ sidewall passivation to produce high aspect ratio structures. Yeh demonstrated patterning fine features (~2.5 μm) in thin films but observed an etch selectivity near unity between Parylene C and photoresist by RIE [29]. Vertical profiles were achieved when using metal or oxide masks and under conditions of low pressure, low power and a biased substrate. However, etched features exhibited significant roughness and the presence of dense micrograss structures due to redeposition of the hard mask [28, 29]. Parylene removal by RIBE achieved smoother surfaces but at the expense of greatly reduced etch rates (~10's of Å min^{-1} compared to ~10^2–10^3 Å min^{-1}) [27].

Recently sidewall passivation and inductively coupled plasma sources have been explored to achieve anisotropic
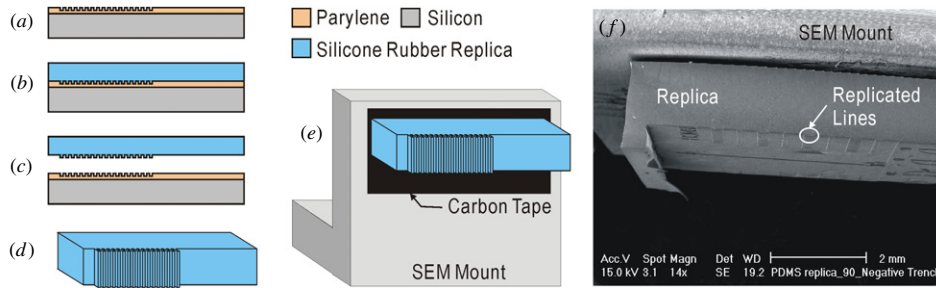
Figure 2. Illustrations (*a*)–(*d*) of the process used to fabricate silicone rubber replicas of etched Parylene C features and (*e*) the replica mounting method in preparation for SEM viewing. (*f*) SEM image of a sectioned silicone rubber replica that has been Au sputter-coated.
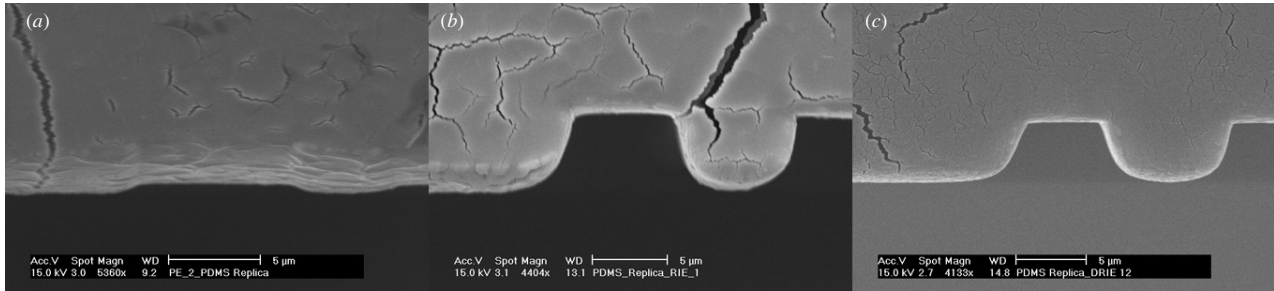

Figure 3. Au-coated cross sections of PDMS replicas of 10 μm line features etched using (*a*) plasma etching, (*b*) RIE and (*c*) DRIE modes. The scale bar in each image measures 5 μm. Cracking of the Au conductive coating is evident.

etching of polymers. Zahn achieved aspect ratios up to 20:1 for deep reactive ion etching (DRIE) of polymethylmethacrylate (PMMA) by using a switched chemistry etching technique inspired by the Bosch process for silicon removal [31]. SiO$_2$ masks and an inductively coupled plasma source were used to create vertical Parylene N sidewalls in high-density oxygen-based plasmas (Ar/O$_2$) [30]. The anisotropy was in part attributed to the sidewall passivation by redeposition of oxygen-deficient etch products which prevent lateral erosion due to reflection of atomic and molecular oxygen. Anisotropy was further improved by increasing the substrate bias which is consistent with the results of earlier studies.

2.3. Alternative methods

Alternative methods for the selective deposition and removal of Parylene insulation layers on implantable electrodes have been reported. The thickness of deposited Parylene is a function of substrate temperature [32, 33] so biased resistors were used to generate a localized heat gradient that prevented deposition in regions held above 70 °C [34]. Parylene has been used as an insulation coating for microelectrodes used in neural recordings. Selective removal by ultraviolet laser ablation [35, 36] and manual mechanical removal on wire microelectrodes [37] has also been reported.

More recently, thermal imprint patterning in Ni molds and micromolding techniques have also been investigated. Thermal imprinting achieved 25 μm high 10 μm wide line features in 30 μm thick parylene, but required high temperature processing at 250 °C to enable accurate pattern replication [38]. Micromolding of Parylene films to a
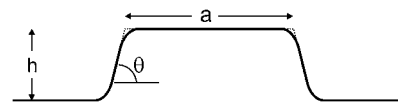

Figure 4. Illustration showing parameters measured to obtain the vertical etch rate, lateral etch rate and sidewall angle.

patterned mold and then thermocompression bonding with a second Parylene film was developed as an alternative to surface micromachining of microchannels [39, 40].

3. Experimental methods

3.1. Preparation of etched Parylene C coupons

Four inch silicon wafers were treated with A-174 silane adhesion promoter (Specialty Coating Systems, Indianapolis, IN). Next, the back side of each wafer was covered with a dicing saw tape (Nitto Denko Corporation, Osaka, Japan) to restrict Parylene coating to only the front side. 10 μm of Parylene C (Specialty Coating Systems, Indianapolis, IN) was deposited (PDS 2010 Labcoter, Specialty Coating Systems, Indianapolis, IN). The Parylene coating was gently scored with a sharp razor and the dicing saw tape was carefully removed from the back side. After priming with hexamethyldisilazane (HMDS), 14 μm of photoresist (AZ 4620, AZ Electronic Materials, Branchburg, NJ) was applied by spin coating (1 krpm for 40 s) and then patterned with an etching calibration pattern consisting of lines, trenches and other geometrical features.
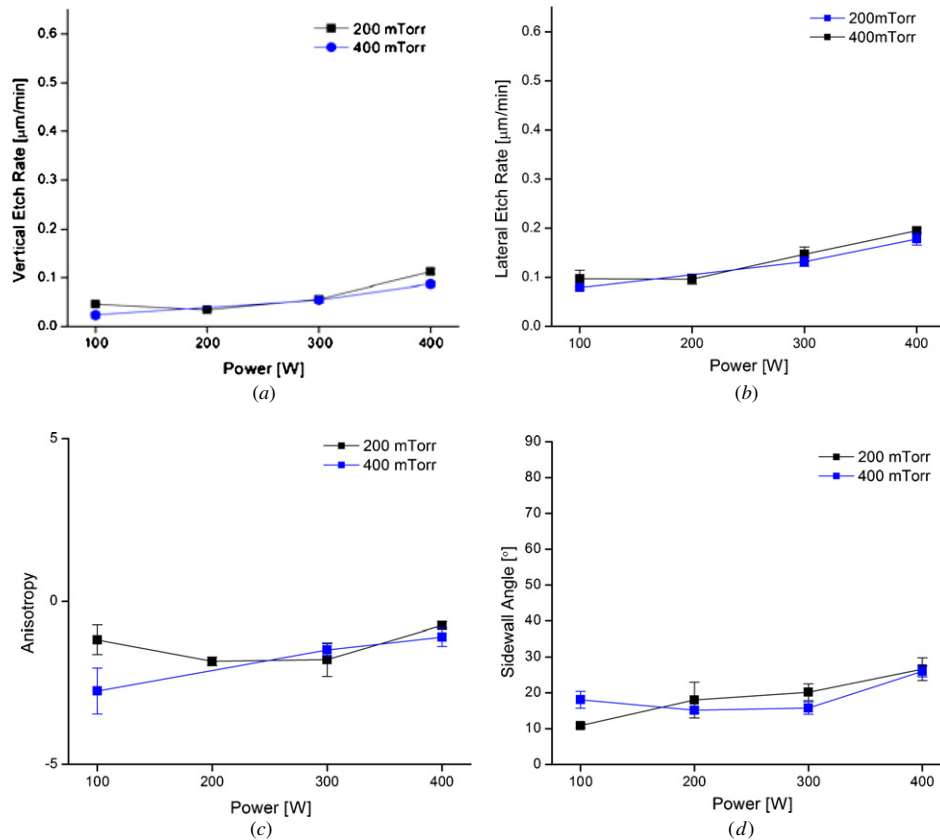
Figure 5. Etch data for Parylene C samples ($n = 4$) processed by plasma etching using oxygen plasma: (*a*) vertical etch rate, (*b*) lateral etch rate, (*c*) anisotropy and (*d*) the measured sidewall angle. Process pressure (200 and 400 mTorr) and power (100, 200, 300 and 400 W) were varied.

Table 1. Process parameters examined in each of the etching modes.

Plasma etching	Reactive ion etching	Deep reactive ion etching
Power	Power	Power
Pressure	Pressure	Pressure
	O_2 flow rate	O_2 flow rate
		Addition of Ar
		Sidewall passivation with C_4F_8
		Etch step time

Patterned test coupons measuring 20 mm × 10 mm and containing two identical calibration dies were carefully separated from wafers by manually scribing and breaking each piece. Test coupons were etched for a fixed time of 10 min under varying process conditions in plasma etching (PEII-A, Technics Plasma, Kirchheim, Germany), RIE (1000 TP/CC, SemiGroup Texas, LLC, McKinney, Texas), and DRIE (PlasmaTherm SLR-770B, Unaxis Corporation, St Petersburg, FL) equipment. Process pressure, gas flow, power and etching chemistries were varied. DRIE mode enabled switched chemistry etching in which samples were exposed to alternating cycles of (1) deposition of a C_4F_8-based Teflon-like sidewall passivation layer and (2) etching in O_2 plasma. Deposition of the fluoropolymer layer protected the sidewalls from lateral etching. Table 1 summarizes the process

parameters examined in each etching mode. Table 2 shows in detail the process recipes used in DRIE of Parylene C. One test coupon was processed for each condition examined. For plasma etching, 8 different process conditions were studied. RIE and DRIE studies involved 18 and 21 different process conditions. In total, 47 test coupons were processed (94 dies, 2 dies each process condition).

3.2. Photoresist mask etch rate measurement

The step heights of the etched structures (photoresist + Parylene) were measured using a surface profilometer (Alpha-Step 200, KLA-Tencor, San Jose, CA). Then the two dies in each test coupon were separated manually by scribing and breaking. The remaining photoresist was removed on one of the dies. The step heights of the remaining Parylene structures were measured. The obtained step height data were used to calculate the vertical etch rates of the photoresist masking layer.

3.3. Preparation of SEM samples by replica molding

Accurate determination of vertical etch rate, lateral etch rate, sidewall angle and the etch profile is possible only by examining cross-section samples under scanning electron microscopy (SEM). Preparation of Parylene samples for SEM
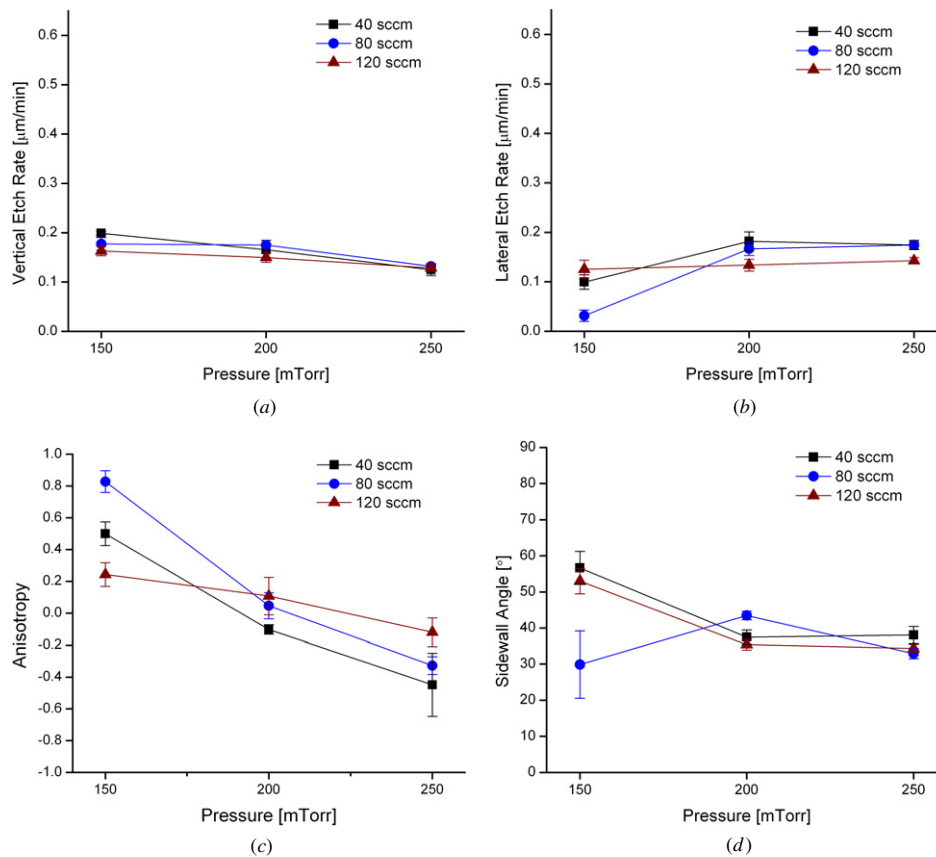
Figure 6. Etch data for Parylene C samples ($n = 4$) processed by RIE using an oxygen plasma at 200 W: (*a*) vertical etch rate, (*b*) lateral etch rate, (*c*) anisotropy and (*d*) the measured sidewall angle. Process pressure (150, 200 and 250 mTorr) and oxygen flow rate (40, 80 and 120 sccm) were varied.

Table 2. Parameters for DRIE recipes.

Recipe parameters	Oxygen only	Oxygen + argon	Switched chemistry
O_2 flow rate (sccm)	20, 60, 100	20, 60, 100	20, 60, 100
C_4F_8 flow rate (sccm)	0	0	35
Ar flow rate (sccm)	0	0, 50, 100	(40, during the deposition step)
Etch coil power (W)	400, 800	800	800
Etch platen power (W)	20	20	20
Deposition coil power (W)	N/A	N/A	825
Deposition platen power	N/A	N/A	1
Etch step time (s)	600	600	10, 20
Deposition time (s)	N/A	N/A	3
Etch process pressure (mTorr)	13, 23	23	23
Deposition process pressure (mTorr)	N/A	N/A	22

is particularly challenging. In general, cleaving polymer films to produce cross-sections requires special techniques, such as focused ion beam (FIB) or cryogenic freezing, to prevent tearing or deformation of fine features. However, consistent cross-sections of Parylene films are difficult to obtain by cleaving frozen samples and FIB tools are both rare and expensive. Accurate negative reproductions of delicate etched features can be obtained by replication, a method commonly employed in polymer microscopy [41]. Application of replica casting allowed preparation of cross sections of etched structures in a non-destructive manner.

The replication process is summarized in figure 2. Silicone rubber (Sylgard 184, Dow Corning, Midland, MI) was prepared (AR-250 Hybrid Mixer, Thinky Corp., Tokyo, Japan) with a 10:1 base-to-curing-agent ratio. The prepolymer mix was poured onto the etched test coupons (figure 2(*a*)), degassed (V0914 vacuum oven, Lindberg/Blue, Asheville, NC), and cured at 65 °C for 1 h (figure 2(*b*)). Each replica was peeled from the etched master and cut into a suitable size for SEM imaging (figure 2(*c*)). Replicas were then cross sectioned with a razor blade (figure 2(*d*)) and sputter-coated with Au, making the surface conductive for SEM viewing (figures 2(*e*) and (*f*)).
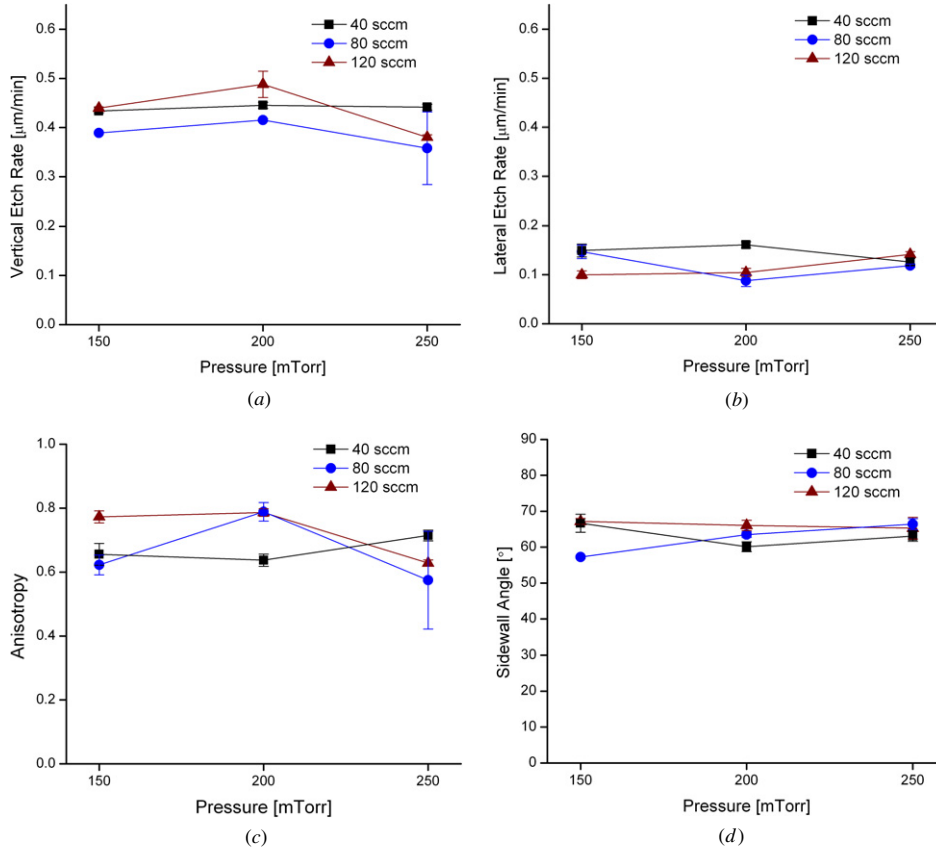
Figure 7. Etch data for Parylene C samples ($n = 4$) processed by RIE using oxygen plasma at 400 W: (*a*) vertical etch rate, (*b*) lateral etch rate, (*c*) anisotropy and (*d*) the measured sidewall angle. Process pressure (150, 200 and 250 mTorr) and oxygen flow rate (40, 80 and 120 sccm) were varied.

3.4. Parylene C etch rate measurement

Replications of etched 10 μm line features for each etching mode are shown in figure 3. The cracks in the image are present in the sputter-coated Au layer and are possibly due to slight expansion in the silicone rubber under vacuum. ImageJ (v.1.34, National Institutes of Health) software facilitated the measurement of individual feature dimensions used in the calculation of vertical etch rate, lateral etch rate and anisotropy. The sidewall angle of etched lines was also obtained from acquired SEM images using ImageJ. Four cross sections of 10 μm line features were measured to obtain these parameters. The definitions for the measurements used to calculate each parameter are defined in figure 4.

Vertical etch rate, R_{vertical}, is defined as

$$R_{\text{vertical}} = \frac{h}{t} \qquad (1)$$

where h is the etched depth and t is the etch duration (10 min in all cases). Lateral etch rate, R_{lateral}, is defined as

$$R_{\text{lateral}} = \frac{(10 \ \mu\text{m} - a)/2}{t} \qquad (2)$$

where a is the width of the top of the etched line. The starting line width was 10 μm for all cases. Etch anisotropy, A, can by quantified by using the following definition [42]:

$$A = 1 - \frac{R_{\text{lateral}}}{R_{\text{vertical}}}. \qquad (3)$$

A vertical profile corresponds to $A = 1$ and occurs when there is no undercutting. The sidewall angle, θ, is measured as indicated in figure 4.

4. Results and discussion

The lateral and vertical etch rates, anisotropy, and sidewall angle of 10 μm wide Parylene C lines obtained by oxygen plasma removal in each etching mode as functions of applied power and process pressure were determined (figures 5–8). In the RIE and DRIE modes, the effect of varying the oxygen flow rate was also examined. All of the data presented in these plots are displayed as mean $\pm$ SE where $n = 4$. Representative SEM images for Parylene C removal by oxygen-only plasmas in each of the different etching systems are presented in figure 9.

As expected for plasma etching, the vertical and lateral etch rates were similar; in some cases, the lateral etch rate was greater than the vertical etch rate (figure 5). The etched profiles of Parylene C lines were decidedly isotropic. Changing the process pressure did little to affect the vertical etch rate but seemed to provide a slight improvement in sidewall angle. At 400 mTorr and 200 W, the etched lines were damaged and only two line samples were recovered. Since the sample size was
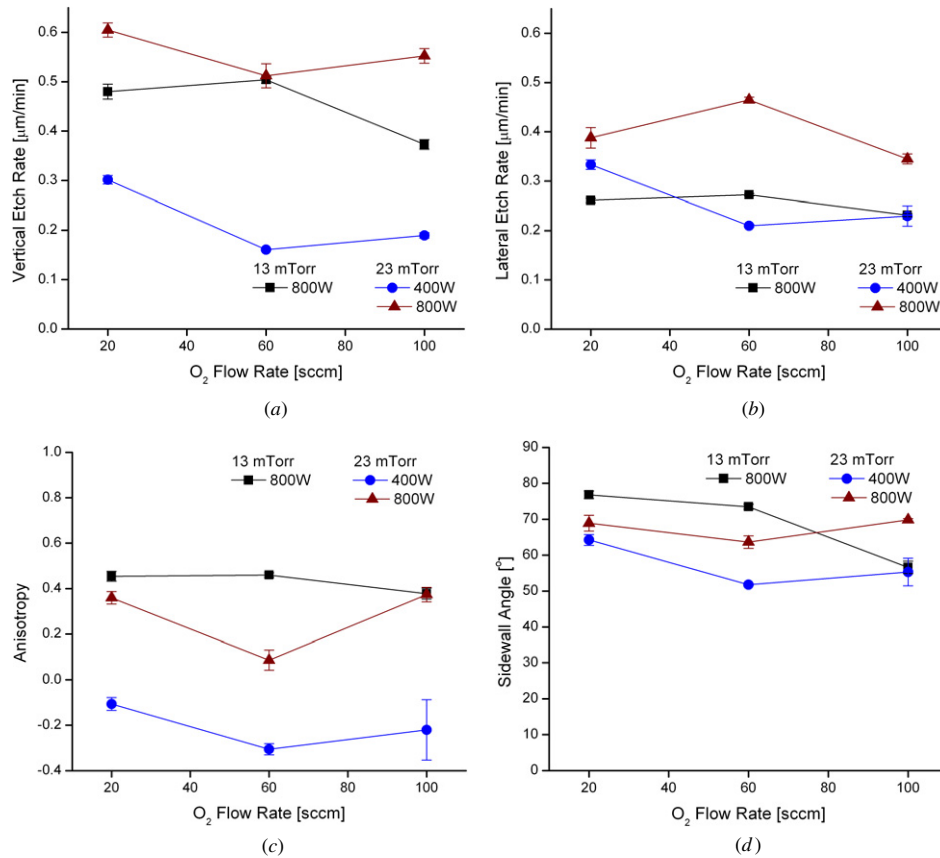
Figure 8. Etch data for Parylene C samples ($n = 4$) processed by DRIE using oxygen plasma: (*a*) vertical etch rate, (*b*) lateral etch rate, (*c*) anisotropy and (*d*) the measured sidewall angle. Process pressure (13 and 23 mTorr), oxygen flow rate (20, 60 and 100 sccm) and power (400 and 800 W) were varied.

insufficient to perform statistical analysis, the data point was omitted.

For Parylene C coupons etched by RIE, the vertical etch rate increased with increasing power (figures 6, 7). At 200 W, the vertical etch rate decreased as oxygen flow rate and process pressure were increased; whereas at 400 W, the vertical etch rate remained relatively constant. The lateral etch rate was similar at 200 and 400 W. At 200 W, however, the lateral etch rate increased as oxygen flow rate and process were increased. The magnitude of the lateral etch rate was similar to that of the vertical etch rate for these conditions. At higher power (400 W), the ratio of the vertical-to-lateral etch rate was higher resulting in better anisotropy and improved sidewall angles.

Interestingly, although higher anisotropy ($\sim$0.8) was achieved for the 80 sccm O_2 setpoint in the 200 W case, the corresponding sidewall angle was only $\sim$30°. Such conditions are possible upon a closer inspection of the definitions for these parameters given in figure 4 and equations (1)–(3). The lateral etch rate calculation assumes that the starting photoresist mask measured exactly 10 μm in width. Since the actual measurement site varies slightly from sample to sample, the corresponding mask dimension cannot be measured precisely prior to etching. Also, the replica molding technique requires smooth sidewalls making it difficult to monitor mask erosion following etching. In all cases, the photoresist masking layer

was removed prior to replication of etched line features for SEM viewing. In the particular case under examination here, the difference between anisotropy and sidewall angle implies either reduced vertical etching efficiency near the sidewalls or the width of the starting photoresist mask may have been slightly larger than 10 μm.

Higher vertical etch rates ($>$0.5 μm min^{-1}) were possible with DRIE using an oxygen-only plasma but with corresponding increases in lateral etch rates as well. The vertical and lateral etch rates tended to increase with increasing power and process pressure and decreasing oxygen flow rate (figure 8). At 800 W, the ratio of the vertical-to-lateral etch rate was greater, yielding clear advantages in anisotropy and sidewall angle over the 400 W case. In comparison to RIE, the DRIE mode yielded slightly better sidewall angles. Surprisingly, the vertical etch rate was not significantly greater than the lateral etch rate at 400 W. Given the operating mechanism behind DRIE, this trend was not expected and further experiments are required to fully understand the nature of this effect.

The etch rate for polymers generally increases with oxygen gas pressure (flow limited regime) and decreases for higher pressure where the active species can be removed before it can react [23]. It has also been suggested that the maximum etch rate corresponds to the maximum oxygen
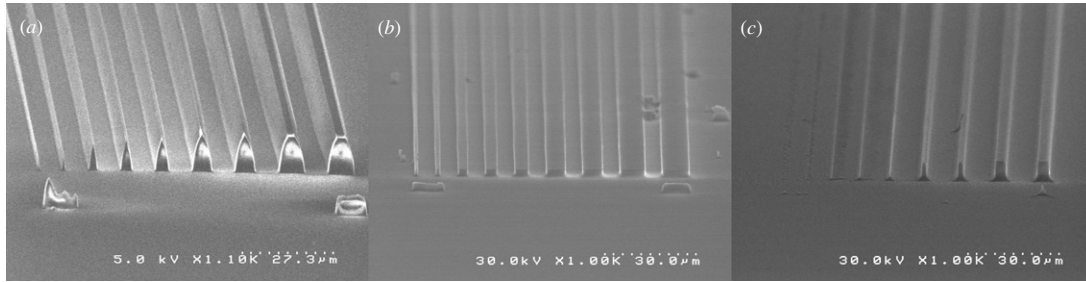
Figure 9. Representative SEM images of etched Parylene C lines produced by (*a*) plasma etching (400 mTorr, 400 W), (*b*) RIE (150 mTorr, 20 sccm, 400 W) and (*c*) DRIE (23 mTorr, 100 sccm, 800 W) with oxygen-only plasmas. The photoresist masking layer was removed and samples were coated in Au to prevent charging; (*a*) and (*c*) were reprinted with permission (© 2005 IEEE) [43].
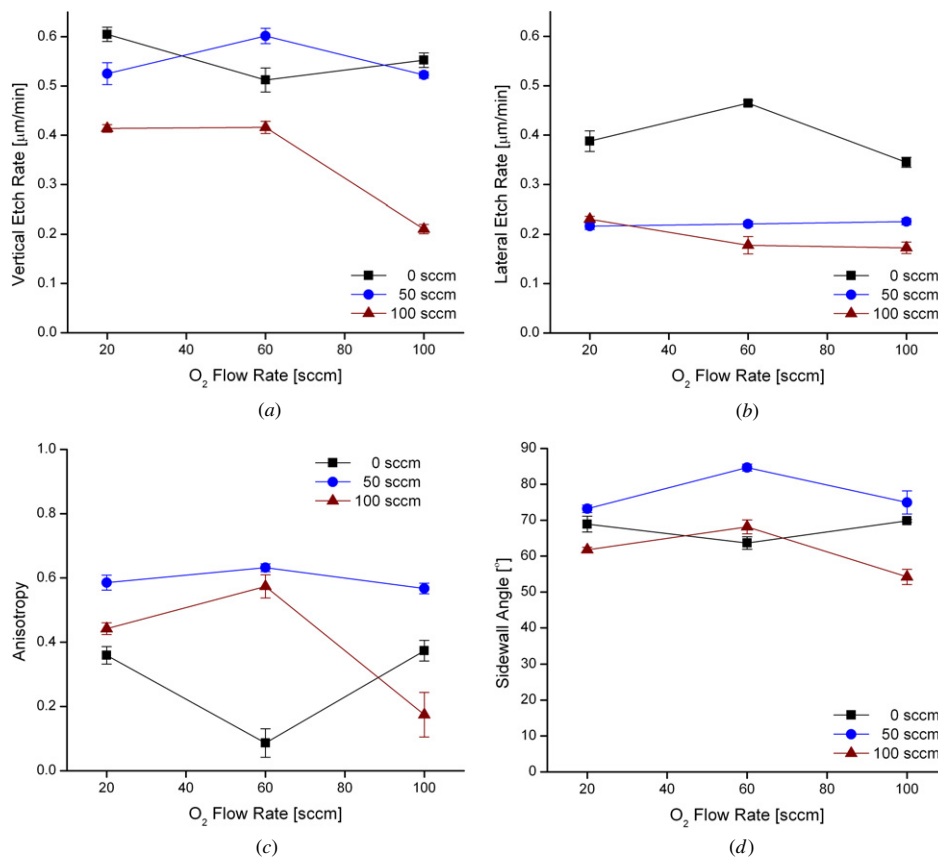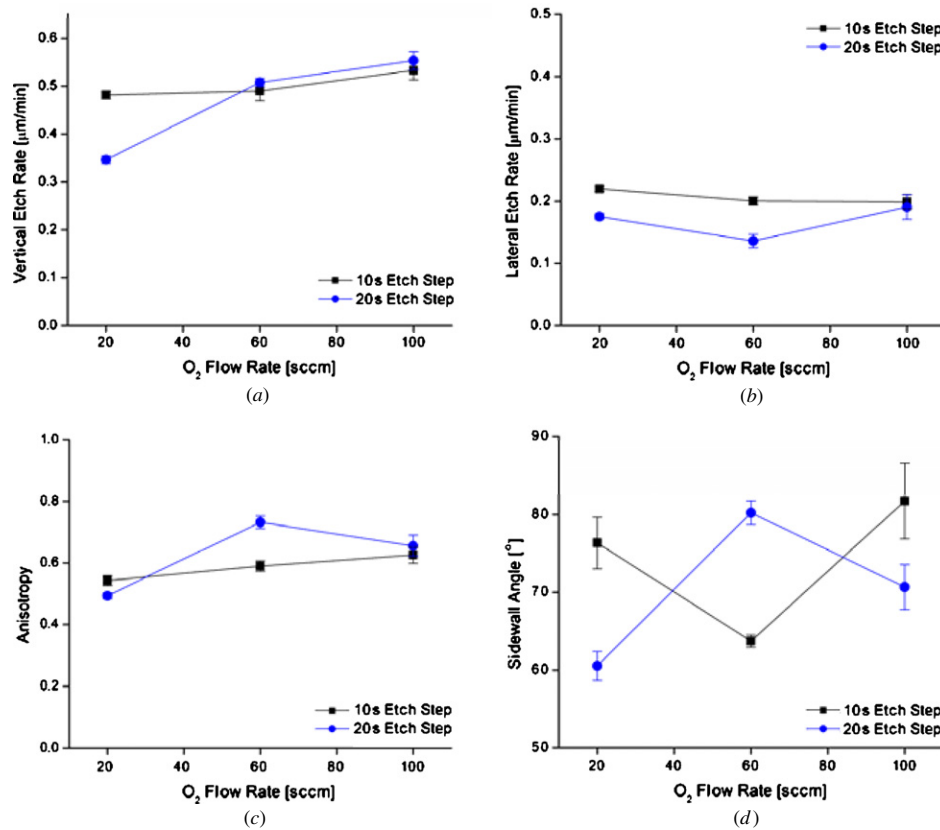

Figure 10. Etch data for Parylene C samples processed by DRIE using oxygen and argon plasma: (*a*) vertical etch rate, (*b*) lateral etch rate, (*c*) anisotropy and (*d*) the measured sidewall angle. The oxygen flow rate (20, 60 and 100 sccm) and argon flow rate (0, 50 and 100 sccm) were varied. The process pressure was 23 mTorr and the applied power was 800 W.

radical concentration and that further increases in gas pressure are accompanied by an increase in the oxygen recombination and reduction in oxygen radical concentration [24]. Hence, it is reasonable that the addition of CF_4 to the oxygen plasma has been shown to enhance Parylene etching [28]. A similar technique is used in photoresist etching in which few percent CF_4 is added to the oxygen plasma. The addition of fluorine containing gases such as CF_4 and SF_6 is thought to increase oxygen atom concentration compared to a pure O_2 plasma and increase etch rate or to produce HF and leave unsaturated

or radical sites for oxygen atom attack [22, 44, 45]. Other gases may also improve Parylene etching; the addition of N_2 to oxygen plasma contributes to increase O atom generation and the addition of He increases electron densities and energies in the plasma [22]. In the studies presented here, additional gas lines were not available on all the process tools for further investigation of the described effects.

In the DRIE mode, the effects of adding argon to the oxygen plasma and the use of switched chemistry etching were also examined. The lateral and vertical etch rates, anisotropy,

Figure 11. Etch rates for Parylene C samples processed by DRIE using switched chemistry etching: (*a*) vertical etch rate, (*b*) lateral etch rate, (*c*) anisotropy and (*d*) the measured sidewall angle. The oxygen flow rate (20, 40 and 100 sccm) was varied and two different etch step durations (10 and 20 s) were examined. The process pressure was 23 mTorr and the applied power was 800 W.
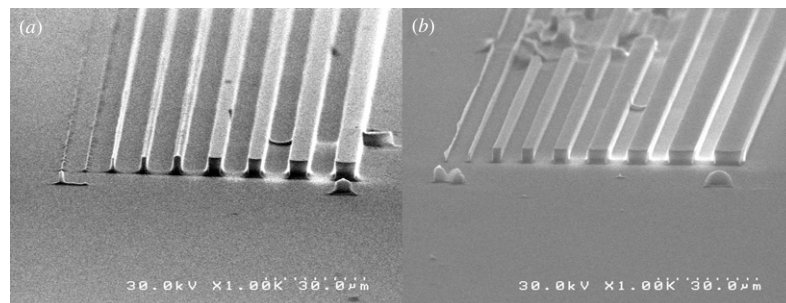
Figure 12. Representative SEM images of DRIE Parylene C lines produced by (*a*) oxygen and argon plasma (23 mTorr, 20 sccm O_2, 50 sccm Ar, 800 W) and (*b*) switched chemistry etching (23, mTorr, 20 sccm O_2, 800 W, 10 s etch step). The photoresist masking layer has been removed and samples coated in Au to prevent charging. The images were reprinted with permission (© 2005 IEEE) [43].

and sidewall angle of 10 μm wide Parylene C lines obtained as a function of oxygen and argon flow rate are shown in figure 10. For switched chemistry etching, the data are displayed in figure 11 as a function of oxygen flow rate and for two different etch step times. A total of 30 and 60 etch loops were performed under switched chemistry etching corresponding to etch step times of 10 and 20 s, respectively, for a total fixed etch time of 10 min. The deposition step time was held constant at 3 s. The representative SEM images of etched Parylene C lines in these process conditions are presented in figure 12.

Ion bombardment can reportedly lower the activation energy for etching some polymers [22]. In this case, the addition of Ar unexpectedly reduces the vertical and lateral etch rates. It is possible that energetic bombardment of the Parylene surface by Ar induces damage that may result in formation of a cross-linked, etch resistant layer [30]. At 50 sccm Ar, sidewall angle improvement was obtained. However, at 100 sccm Ar, sidewall angles fell below that corresponding to the oxygen-only case.

Switched chemistry etching resulted in some of the best etch profiles and sidewall angles compared to the other process

Table 3. Summary of etch recipes in each of the different etching modes.

	Highest vertical etch rate		Lowest lateral etch rate		Best anisotropy		Best sidewall angle	
	Value (μm min^{-1})	Process conditions	Value (μm min^{-1})	Process conditions	Value (μm min^{-1})	Process conditions	Value ($°$)	Process conditions
Plasma etching	0.11 ± 0.01	400 W 200 mTorr	0.08 ± 0.00	100 W 400 mTorr	-0.74 ± 0.12	400 W 200 mTorr	26.62 ± 3.19	400 W 400 mTorr
Reactive ion etching	0.49 ± 0.03	400 W 200 mTorr 120 sccm	0.03 ± 0.01	200 W 150 mTorr 80 sccm	0.83 ± 0.07	200 W 150 mTorr 80 sccm	67.16 ± 0.81	400 W 150 mTorr 120 sccm
Deep reactive ion etching (O_2)	0.60 ± 0.01	800 W 23 mTorr 20 sccm	0.21 ± 0.00	400 W 23 mTorr 60 sccm	0.46 ± 0.01	800 W 13 mTorr 60 sccm	76.80 ± 1.04	800 W 13 mTorr 20 sccm
Deep reactive ion etching (O_2+Ar)	0.60 ± 0.02	800 W 23 mTorr 60 sccm O_2 50 sccm Ar	0.17 ± 0.01	800 W 23 mTorr 100 sccm O_2 100 sccm Ar	0.63 ± 0.01	800 W 23 mTorr 60 sccm O_2 50 sccm Ar	84.66 ± 0.98	800 W 23 mTorr 60 sccm O_2 50 sccm Ar
Deep reactive ion etching (switched chemistry)	0.55 ± 0.02	800 W 23 mTorr 100 sccm O_2 20 s	0.14 ± 0.01	800 W 23 mTorr 60 sccm O_2 20 s	0.73 ± 0.02	800 W 23 mTorr 60 sccm O_2 20 s	81.71 ± 4.85	800 W 23 mTorr 100 sccm O_2 10 s

conditions tested. The vertical etch rate increased with increasing flow rate, while the lateral etch rate remained relatively constant over the various processing conditions. It is important to note that the etch rate data do not account for time required to remove the fluorocarbon passivation layer so the actual Parylene C etch rate may in fact be higher. The etch results obtained by switched chemistry are comparable to the best results achieved by RIE. Further optimization of aspect ratios using RIE and DRIE may be possible by examining the effects of substrate bias and other etching chemistries (addition of fluorine containing gases, N_2 or He).

High magnification examination of silicone rubber replicas was performed under SEM; however, sidewall scallops typically observed after DRIE of Si features were not apparent. It is possible that the replica molds are unable to reproduce these nanometer-size features or that the Au conductive coating obscures them. High magnification SEM examination of the sidewalls of etched Parylene C lines was not possible due to charging-induced image degradation.

Photoresist etch rates for the various etch modes were previously presented and are not presented here [43]. In general, photoresist is removed at similar rates to that of Parylene C and thus etch selectivity is not optimal, especially when etching thick (>10 μm) Parylene C layers is required. Other masks such as sputtered *a*-silicon, sputtered oxide and aluminum were also examined. The sputtered films exhibited poor adhesion to the underlying Parylene C films during etching. During switched chemistry etching, *a*-silicon films were attacked during the fluoropolymer deposition step. Etched Parylene C films masked by *a*-silicon exhibited rough surfaces possibly caused by micromasks formed during the etching process (figure 13). Al masks were plagued by mask sputtering and redeposition [46]. Spin-on glass and nitride masks have been reported in the literature but with only
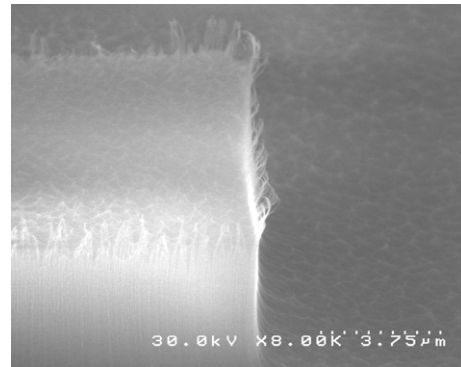
Figure 13. Representative SEM image of the Parylene C line produced by switched chemistry etching. A 0.5 μm thick *a*-silicon etch mask was used, however, the mask was attacked during the fluoropolymer deposition step and only small remnants of the mask remain in the form of thin filaments attached to the top outline of the etched line (image courtesy of Dr Seiji Aoyagi).

limited success [30]. Recently, Miserendino and Tai have demonstrated that Parylene C can be patterned with an SU-8 mask although the masking material was not removed after etching [47].

Using the recipes developed here, aspect ratios of at least 2:1 can be achieved in both RIE and DRIE modes. Oxygen plasma etching is limited to ratios of 1:1. Furthermore, tuning of the sidewall profile (tapered, vertical or reentrant) is possible with DRIE. The optimal process conditions for each mode of Parylene C etching are summarized in table 3. In figure 14, SEM images of Parylene C structures fabricated using switched chemistry DRIE are shown. The corresponding etching recipe is provided in table 4. Each etch cycle consisted of three steps: (1) deposition of a C_4F_8-based Teflon-like
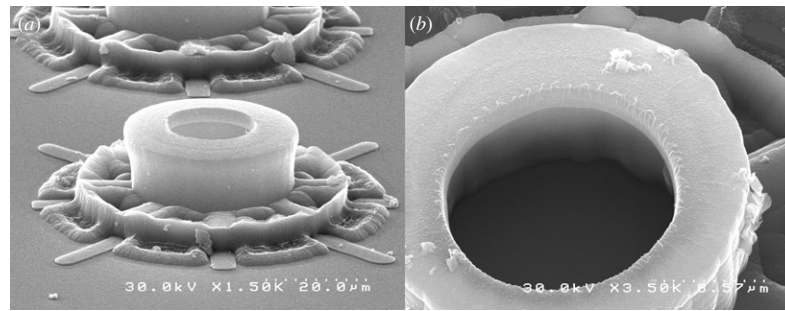
Figure 14. SEM image of (*a*) Parylene C neurocages and (*b*) close-up of chimney opening at the top of the cage etched using the DRIE switched chemistry recipes developed.

Table 4. Switched chemistry etching recipe to produce Parylene C neurocages.

Recipe parameters	
O_2 flow rate (sccm)	60
SF_6 flow rate (sccm)	50
C_4F_8 flow rate (sccm)	35
Ar flow rate (sccm)	40, for all steps
Etch coil power (W)	825
Etch platen power (W)	9 (SF_6), 20 (O_2)
Deposition coil power (W)	825
Deposition platen power	1
SF_6 etch step time (s)	3
O_2 etch step time (s)	10
Deposition time (s)	3
Etch process pressure (mTorr)	23
Deposition process pressure (mTorr)	22

sidewall passivation layer, (2) etching in SF_6 plasma and (3) etching in O_2 plasma. A short SF_6 etch step was added and thought to facilitate removal of the deposited fluoropolymer layer. A 14 μm thick AZ 4620 mask was used and a Parylene C etch rate of 0.33 ± 0.01 μm min^{-1} ($n = 3$) was obtained [16]. Again, the actual etch rate of Parylene C may be higher as the calculated rate does not account for the time consumed to remove the deposited fluoropolymer layer. These structures are neurocages and serve to house embryonic neurons cultured in artificial patterned arrays. The cages require anisotropic etching of Parylene C to produce the openings in the chimney on top of the cage and also to expose the tunnels radiating from the base of each cage. Vertical sidewalls were produced.

Recently, Selvarasah *et al* have shown that up to 55 μm of Parylene C can be etched using an Al mask [46]. This was achieved by reducing the etch temperature. Vertical sidewalls, aspect ratios of at least 8:1 and etch rates of 0.5–1.7 μm min^{-1} were achieved. However, during the etching process, sputtering of the Al mask left residue on the etch features which had to be removed in an additional processing step. Interestingly enough, it has been reported that the etch rate increases with temperature for Parylene N [24]. Here, temperature was not controlled or monitored due to limitations of the etching equipment.

5. Conclusion

Selective Parylene C removal was investigated and characterized using several dry etching methods including plasma etching, RIE and DRIE techniques. Switched chemistry recipes in the DRIE mode were also investigated. In these studies, oxygen was used as the primary reactive species. Replica casting was applied to create cross sections of etch structures for SEM viewing. From these images, vertical etch rates, lateral etch rates, anisotropy and sidewall angles were determined for each of the methods. These results establish trend lines for several distinct Parylene C plasma removal processes and provide a starting point for developing new recipes. Application of developed etch recipes to the fabrication of complex Parylene C microstructures such as neurocages was demonstrated. Selective Parylene C removal will further facilitate its use as a structural material in MEMS in other biomedical and lab-on-a-chip applications.

References

[1] Kroschwitz J I 1998 *Kirk-Othmer Encyclopedia of Chemical Technology* (New York: Wiley)
[2] Szwarc M 1947 Some remarks on the ch2=benzene=ch2 molecule *Discuss. Faraday Soc.* **2** 46–9
[3] Specialty Coating Systems *Parylene knowledge > discovery/ history* (available from http://www.scscoatings. com/parylene_knowledge/history.aspx)
[4] Gorham W F 1966 A new general synthetic method for preparation of linear poly-*p*-xylylenes *J. Polym. Sci. Polym. Chem. Ed.* **4** 3027–39
[5] Wolgemuth L 2006 Crystal-clear coating covers components *Med. Des.* **6** 48–51

[6] Wang X Q and Tai Y C 2000 A normally closed in-channel micro check valve *13th IEEE Int. Conf. on Micro Electro Mechanical Systems, 2000 (Miyazaki, Japan, 23–27 Jan. 2000)* (Piscataway, NJ: IEEE) pp 68–73

[7] Xie J, He Q, Tai Y-C, Liu J and Lee T 2002 Integrated electrospray chip for mass spectrometry *7th Int. Conf. on Min. Chem. and Biochem. Anal. Sys.: Proc. mTAS 2002 (Nara, Japan, 3–7 Nov. 2002)* (Dordrecht: Kluwer) pp 709–11

[8] Xie J, Miao Y N, Shih J, Tai Y C and Lee T D 2005 Microfluidic platform for liquid chromatography-tandem mass spectrometry analyses of complex peptide mixtures *Anal. Chem.* **77** 6947–53

[9] Yang X, Yang J M, Tai Y C and Ho C M 1999 Micromachined membrane particle filters *Sensors Actuators* A **73** 184–91

[10] Yao T J, Yang X and Tai Y C 2002 Brf3 dry release technology for large freestanding parylene microstructures and electrostatic actuators *Sensors Actuators* A **97–98** 771–5

[11] Tai Y C 2003 Parylene for mems applications *Abstracts of Papers of the American Chemical Society (New York, 7–11 Sept. 2003)* (Blacksburg, VA: American Chemical Society) vol 226 p U360

[12] Lahann J 2006 Vapor-based polymer coatings for potential biomedical applications *Polym. Int.* **55** 1361–70

[13] Weisenberg B A and Mooradian D L 2002 Hemocompatibility of materials used in microelectromechanical systems: platelet adhesion and morphology *in vitro J. Biomed. Mater. Res.* **60** 283–91

[14] He Q, Meng E, Tai Y-C, Rutherglen C M, Erickson J and Pine J 2003 Parylene neuro-cages for live neural networks study *Transducers 2003 (Boston, MA)* pp 995–8

[15] Tooker A, Meng E, Erickson J, Tai Y C and Pine J 2005 Biocompatible parylene neurocages *IEEE Eng. Med. Biol. Mag.* **24** 30–3

[16] Meng E, Tai Y-C, Erickson J and Pine J 2003 Parylene technology for mechanically robust neuro-cages *7th Int. Conf. on Min. Chem. Biochem. Anal. Sys.: Proc. mTAS 2003 (Squaw Valley, CA, 5–9 Oct. 2003)* vol 2 (Cleveland Heights, OH: Transducers Research Foundation) pp 1109–12

[17] Takeuchi S, Ziegler D, Yoshida Y, Mabuchi K and Suzuki T 2005 Parylene flexible neural probes integrated with microfluidic channels *Lab Chip* **5** 519–23

[18] Lahann J, Klee D, Thelen H, Bienert H, Vorwerk D and Hocker H 1999 Improvement of haemocompatibility of metallic stents by polymer coating *J. Mater. Sci. Mater. Med.* **10** 443–8

[19] Nowlin T E and Smith D F Jr 1980 Surface characterization of plasma-treated poly-*p*-xylylene films *J. Appl. Polym. Sci.* **25** 1619–32

[20] Herrera-Alonso M and McCarthy T J 2004 Chemical surface modification of poly(*p*-xylylene) thin films *Langmuir* **20** 9184–9

[21] Specialty Coating Systems 2001 *Solvent Resistance of Parylene*

[22] Egitto F D, Vukanovic V and Taylor G N 1990 Plasma etching of organic polymers *Plasma Deposition, Treatment, and Etching of Polymers* ed R d'Agostino (San Diego, CA: Academic) pp 322–412

[23] Callahan R R A, Pruden K G, Raupp G B and Beaudoin S P 2003 Downstream oxygen etching characteristics of polymers *J. Vac. Sci. Technol.* B **21** 1496–500

[24] Callahan R R A, Raupp G B and Beaudoin S P 2001 Effects of gas pressure and substrate temperature on the etching of parylene-n using a remote microwave oxygen plasma *J. Vac. Sci. Technol.* B **19** 725–31

[25] Wang X-Q, Lin Q and Tai Y-C 1999 A parylene micro check valve *12th IEEE Int. Conf. on Micro Electro Mechanical Systems, 1999 (Orlando, FL, 17–21 Jan. 1999)* (Piscataway, NJ: IEEE) pp 177–82

[26] Levy B P, Campbell S L and Rose T L 1986 Definition of the geometric area of a microelectrode tip by plasma-etching of parylene *IEEE Trans. Bio-Med. Eng.* **33** 1046–9

[27] Ratier B, Jeong Y S, Moliton A and Audebert P 1999 Vapor deposition polymerization and reactive ion beam etching of poly(*p*-xylylene) films for waveguide applications *Opt. Mater.* **12** 229–33

[28] Majid N, Dabral S and McDonald J F 1989 The parylene–aluminum multilayer interconnection system for wafer scale integration and wafer scale hybrid packaging *J. Electron. Mater.* **18** 301–11

[29] Yeh J T C and Grebe K R 1983 Patterning of poly-*para*-xylylenes by reactive ion etching *J. Vac. Sci. Technol.* A **1** 604–8

[30] Standaert T E F M *et al* 2001 High-density plasma patterning of low dielectric constant polymers: a comparision between polytetrafluoroethylene, parylene-n, and poly(arylene ether) *J. Vac. Sci. Technol.* A **19** 435–46

[31] Zahn J D, Gabriel K J and Fedder G K 2002 A direct plasma etch approach to high aspect ratio polymer micromachining with applications in biomems and CMOS-MEMS *15th IEEE Int. Conf. on Micro Electro Mechanical Systems, 2002 (Las Vegas, Nevada, 20–24 Jan. 2002)* (Piscataway, NJ: IEEE) pp 137–40

[32] Kramer P, Sharma A K, Hennecke E E and Yasuda H 1984 Polymerization of *para*-xylylene derivatives (parylene polymerization): 1. Deposition kinetics for parylene-n and parylene-c *J. Polym. Sci., Polym. Chem. Ed.* **22** 475–91

[33] Gazicki M, Surendran G, James W and Yasuda H 1985 Polymerization of *para*-xylylene derivatives (parylene polymerization): 2. Heat-effects during deposition of parylene-c at different temperatures *J. Polym. Sci., Part A: Polym. Chem.* **23** 2255–77

[34] Sabeti R, Charlson E M and Charlson E J 1989 Selective deposition of parylene *Polym. Commun.* **30** 166–9

[35] Loeb G E, Peck R A and Martyniuk J 1995 Toward the ultimate metal microelectrode *J. Neurosci. Methods* **63** 175–83

[36] Schmidt E M, Bak M J and Christensen P 1995 Laser exposure of parylene-c insulated microelectrodes *J. Neurosci. Methods* **62** 89–92

[37] Lerner H, Zahradnik R T and Buchbinder M 1982 Miniature implantable tantalum tantalum oxide stimulating electrodes *IEEE Trans. Bio-Med. Eng.* **29** 290–2

[38] Youn S W, Goto H, Takahashi M, Ogiwara M and Maeda R 2007 Thermal imprint process of parylene for mems applications *Key Eng. Mater.* **340–1** 931–6

[39] Noh H S, Hesketh P J and Frye-Mason G C 2002 Parylene gas chromatographic column for rapid thermal cycling *J. Microelectromech. Syst.* **11** 718–25

[40] Noh H S, Huang Y and Hesketh P J 2004 Parylene micromolding, a rapid and low-cost fabrication method for parylene microchannel *Sensors Actuators* B **102** 78–85

[41] Sawyer L C and Grubb D T 1996 *Polymer Microscopy* (London: Chapman and Hall)

[42] Manos D M and Flamm D L 1989 *Plasma Etching: An Introduction (Series: Plasma–Materials Interactions)* (Boston, MA: Academic)

[43] Meng E and Tai Y-C 2005 Parylene etching techniques for microfluidics and biomems *18th IEEE Int. Conf. on Micro Electro Mechanical Systems, 2005 (Miami, FL, 30 Jan.– 3 Feb. 2005)* (Piscataway, NJ: IEEE) pp 568–71

[44] Flamm D and Donnelly V M 1984 The design of plasma etchants *Plasma Chem. Plasma* P **1** 317–63

[45] Lieberman M A and Lichtenberg A J 1994 *Principles of Plasma Discharges and Materials Processing* (New York: Wiley)

[46] Selvarasah S *et al* 2007 A high aspect ratio, flexible, transparent and low-cost parylene-c shadow mask technology for micropatterning applications *14th Int. Conf. on Solid-State Sensors, Actuators and Microsystems: Proc. Transducers '07 and Eurosensors XXI (Lyon, France, 10–14 June 2007)* (Piscataway, NJ: IEEE) vol 1 pp 533–6

[47] Miserendino S and Tai Y C 2007 Photodefinable silicone mems gaskets and o-rings for modular microfluidic systems *20th IEEE Int. Conf. on Micro Electro Mechanical Systems, 2007 (Kobe, Japan, 21–25 Jan. 2007)* (Piscataway, NJ: IEEE) pp 369–72